ACADEMIC PRESS

Available online at www.sciencedirect.com
SCIENCE DIRECT®

Journal of Catalysis 219 (2003) 107–116

JOURNAL OF CATALYSIS

www.elsevier.com/locate/jcat

The influence of surface properties on the photocatalytic activity of nanostructured TiO_2

King Lun Yeung,[a,*] Sze Tai Yau,[a] A. Javier Maira,[b] Juan M. Coronado,[b] Javier Soria,[b] and Po Lock Yue [a]

[a] *Department of Chemical Engineering, the Hong Kong University of Science and Technology, Clear Water Bay, Kowloon, Hong Kong, SAR China*
[b] *Instituto de Catálisis y Petroleoquímica, CSIC, Campus UAM, Cantoblanco, Madrid 28047, Spain*

Received 23 October 2002; revised 31 March 2003; accepted 10 April 2003

Abstract

Nanostructured TiO_2 with 11- (P11) and 5-nm (P5) crystal sizes were prepared by a modified sol–gel method. Controlled crystallization and a pretreatment process were employed to obtain TiO_2 with different surface roughness and degree of hydroxylation, while maintaining an identical crystal (i.e., 11 or 5 nm) and aggregate (i.e., 100 nm) sizes, phase structure (i.e., anatase), and crystallinity (i.e., X-ray diffraction peak intensity). Using the photooxidation of airborne trichloroethylene as a probe reaction, we were able to identify that the hydroxyl groups on low-coordinated titanium atoms are responsible for the generation of dichloroethylene and dichloroacetaldehyde by-products. Their presence usually means lower TCE conversion and in some cases leads to catalyst deactivation.

1. Introduction

Photocatalytic oxidation (PCO) is an attractive method for low-temperature remediation of volatile organic compounds (VOCs) in process air stream [1–3]. Using inexpensive TiO_2 catalysts irradiated with UV light, airborne VOCs can be mineralized into carbon dioxide, water, and mineral compounds (e.g., HX, where X = Cl) at room temperature. The semiconductor TiO_2 catalyst generates electrons and holes with the absorption of UV photons and these photogenerated charges can migrate toward the catalyst surface where they initiate redox reactions that oxidize the adsorbed organic molecules. The low quantum yield and the possible formation of undesirable by-products are two of the most important issues in PCO technology [4]. Recently, new types of photocatalysts based on nanostructured TiO_2 have been developed in order to address these problems. These nanometer-sized TiO_2 particles exhibited higher activity [5–7] and selectivity [7] than the commercial TiO_2 (P25, Degussa) for gas-phase PCO of VOCs.

Nanostructured TiO_2 with controlled crystal and aggregate sizes were prepared by a modified sol–gel technique [6]. The anatase TiO_2 (3–20 nm) were crystallized from amorphous titania gel spheres by thermal and hydrothermal processes. The nanostructured TiO_2 exhibited different structural, electronic, and catalytic properties, depending on the crystal size [6–9]. A recent study showed that the surface properties of the nanometer-sized TiO_2 catalysts, as well as their photocatalytic activity are affected by the crystallization conditions [10]. This paper attempts to clarify the role of the surface structure and surface hydroxyl groups on the photocatalytic properties of nanostructured TiO_2. Two sets of nanostructured TiO_2 with crystal sizes of 11 nm (P11) and 5 nm (P5) were prepared for the study. Each set of catalysts had similar phase structure (i.e., anatase), crystal (i.e., 11 or 5 nm), and aggregate (i.e., 100 nm) sizes, crystallinity, surface area, and band-gap energy, but differed in their surface properties. Electron paramagnetic resonance (EPR) and Fourier-transformed infrared (FTIR) spectroscopies were used to obtain information on the surface properties of the TiO_2 samples. The photocatalytic oxidation of airborne trichloroethylene was chosen as the probe reaction because of the abundant literature data for this reaction system [11–22]. The photoreaction was monitored by in situ Fourier-transformed infrared spectroscopy.

* Corresponding author.
E-mail address: kekyeung@ust.hk (K.L. Yeung).

0021-9517/$ – see front matter
doi:10.1016/S0021-9517(03)00187-8

2. Experimental

2.1. Synthesis and characterization of nanostructured TiO_2

Nanostructured TiO_2 of well-defined crystal and aggregate sizes were prepared by a modified sol–gel method [6]. The procedure involved the precipitation of amorphous titanium oxide gel spheres, followed by a controlled crystallization of anatase TiO_2 crystals. After thermal or hydrothermal treatments, the amorphous gel spheres were transformed into aggregates of TiO_2 nanocrystals that retained the original size and shape of the gel spheres. By using this method, the aggregate size and shape were fixed, while the primary particle sizes were varied from 3 to 20 nm [6]. Pure anatase and rutile TiO_2 were successfully prepared using this technique. The 11-nm, anatase-TiO_2 were crystallized by thermal (P11t) and hydrothermal (P11h) processes. P11t was obtained by heat treating the 100-nm titania gel spheres in air at 723 K for 3 h, while P11h was synthesized under hydrothermal action at 473 K for 12 h. A third sample, P11h-d was prepared by outgassing P11h in flowing dry air under UV irradiation (fluorescent black lamp, $\lambda = 356$ cm^{-1}) at room temperature (298 K) for 3 h. The 5 nm anatase-TiO_2 (P5h) was crystallized in a solution containing 10 ml isopropanol and 15 ml water at 423 K for 8 h. P5h-d was obtained by outgassing the P5h sample under UV irradiation for 3 h.

The crystal structure, particle size, morphology, and surface area of TiO_2 photocatalysts were characterized using X-ray diffraction (XRD), transmission electron microscopy (TEM) and N_2 physiadsorption. X-ray analyses of the TiO_2 powder were conducted at the Synchrotron Radiation Research Center (SRRC) in Taiwan. The X-ray radiation ($\lambda =$ 1.3271 Å, beam current = 120–200 mA) at beamline BL17A was supplied from a 1.5 GeV storage ring. The XRD patterns were recorded for $15^\circ < 2\theta < 55^\circ$ by step-scanning at 0.05° increments. The phase structure, crystallinity, and grain size of the TiO_2 were determined from the X-ray diffraction pattern. The X-ray absorption spectra of the TiO_2 samples were also obtained at room temperature. Important information on the bond structure (i.e., bond lengths, numbers and types of neighboring atoms) could be obtained from the X-ray absorption data. The transmission spectra were collected using a gas-ionization detector. The ion chambers used for measuring the incident (I_0) and transmitted (I) synchrotron beam intensities were filled with a He/N_2 gas mixture and N_2 gas, respectively. Data were collected from 200 eV below the Ti K-edge (4966 eV) to 1100 eV above the edge. Standard titanium metal foil and commercial anatase TiO_2 were used as reference standards.

The TiO_2 nanoparticles were examined with a Philips CM20 transmission electron microscope at an accelerating voltage of 200 kV. Routine chemical analysis using an in situ energy dispersive X-ray spectrometer (EDXS) detected only the energy signatures corresponding to the Ti and O elements. The average TiO_2 crystal and aggregate sizes, as well as their morphologies, were obtained from the X-ray diffraction peak broadening and TEM micrographs. The BET surface area of the TiO_2 photocatalyst was measured using the N_2 physiadsorption technique (Micromeritics ASAP 2010) after outgassing under vacuum at 523 K for 4 h. The change in the band-gap energy of the TiO_2 as a result of the material preparation was also measured using a Philips/Unicam Pu8700 UV/VIS spectrometer with diffuse and specular reflection accessories to provide information on the electronic band gap. A Ba_2SO_4 standard white plate was used as background. The spectra were recorded at a scan speed of 125 nm/min and a bandwidth of 2 nm.

2.2. Evaluation of photocatalytic activity of TiO_2

Gas phase, photocatalytic oxidation of trichloroethylene (TCE) was conducted in an in situ infrared photoreaction cell. The cell consists of two KBr windows and a sample holder for the catalyst wafer. The reactants and products enter and exit the cell through a set of inlet and outlet ports. The compressed air used in the reaction was metered (800 ml/min) and pretreated through a series of moisture and hydrocarbon traps that included a liquid N_2 trap, a drying column packed with desiccant and molecular sieves. By using a syringe pump (kdScientific 1000), trichloroethylene was fed to a mixing tee where it was vaporized and mixed with the dry air. The reactant mixture then flowed through the in situ IR photoreaction cell and was allowed to equilibrate at room temperature (298 K). Once the reactant concentration had stabilized, the inlet and outlet ports were shut off and the UV lamp was turned on to allow the photoreaction to proceed under batch conditions. The infrared spectra were continuously collected by a Fourier-transform infrared spectrometer (FTS 6000, Bio-Rad Laboratories) during the reaction until the intensity of the characteristic peaks of adsorbed TCE molecule reached a steady state or decreased to a value less than 0.2 of the original. The UV lamp was then turned off and the cell was purged with flowing dry air. The catalyst wafers used in the reaction experiments were prepared by mixing 0.08 g of TiO_2 with 0.70 g of KBr. Three wafers were prepared in each batch and each wafer weighed 0.20 g. The wafer thickness as measured by the scanning electron microscopy (JEOL 6300) was 280 ± 22 μm, thus giving the wafers an average density of 2.28 g/cm^3. The wafers were purged with dry air for 2 h at room temperature to remove adsorbed CO_2.

2.3. Materials

The chemicals used in the synthesis of nanostructured TiO_2 photocatalysts included titanium isopropoxide (97%, Aldrich), 2-propanol (99.5%, Aldrich Chemicals), and distilled water. Standard FTIR-grade potassium bromide (Aldrich Chemicals) was used as the catalyst diluent for the in situ IR experiments. The trichloroethylene (99.5%) used for the catalyst tests was purchased from Aldrich Chemicals. Titanium foils and anatase TiO_2 used as standards for XRD

and XAS experiments were also purchased from Aldrich Chemicals.

3. Results and discussion

3.1. Nanostructured TiO_2

Both sets of P11 and P5 nanostructured TiO_2 prepared by the different crystallization and pretreatment procedures were pure anatase with the TiO_2 crystals forming spherical aggregates of 100 nm in diameter. The average crystal sizes of TiO_2 measured from the X-ray peak broadening were comparable to the results obtained from the micro-Raman spectroscopy, atomic force microscopy, and transmission electron microscopy. Fig. 1a displays the atomic force microscope (Tapping mode, Nanoscope IIIα) image of P5 TiO_2. It is clear from the picture that the individual TiO_2 crystals are about 5 nm in diameter (Fig. 1a, inset) and form spherical aggregates of uniform 100 nm sizes. X-ray photoelectron spectroscopy and EDXS analyses of the surface and bulk compositions of TiO_2 detected only titanium and oxygen, with carbons originating from the organometallic precursors and ambient contamination (i.e., adsorbed CO_2 and hydrocarbons) as the main surface impurity. Table 1 shows that the TiO_2 within each set of samples have comparable crystal size, crystallinity, BET surface area, and UV absorption. In the table, the relative intensity of the anatase (101) peak is used as a qualitative measure of the TiO_2's crystallinity.

The smaller P5 TiO_2 have a larger BET surface area of 220 m^2/g compared to P11 TiO_2 (95 m^2/g). Also, the P5

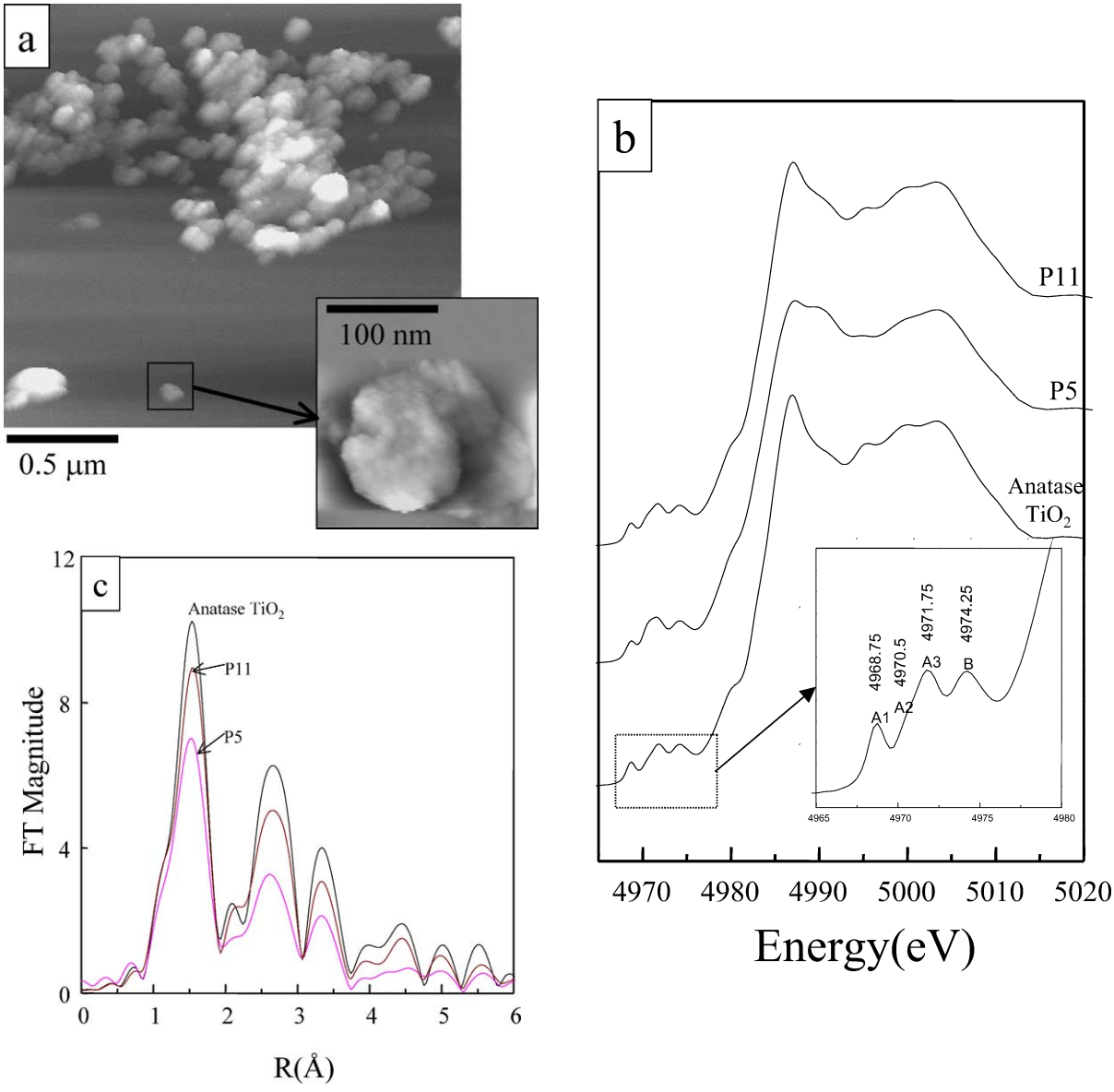

Fig. 1. (a) Atomic force microscope picture of P5 TiO_2, (b) XANES, and (c) EXAFS spectra of nanostructured P5 and P11 TiO_2 along with an anatase TiO_2 standard.

Table 1
Structural, electronic, and catalytic properties of the TiO_2 catalysts

Anatase	Crystal size[b]	Crystallinity[c]	BET area	UV absorption	TCE photooxidation rate ($\times 10^{-9}$ mol^1/s^1 m^2)[d]	
TiO_2[a]	(nm)	I/I_0	(m^2/g)	(nm)	Conversion	Mineralization
P5h	5.1	1	220	388	5.2	3.0
P5h-d	5.1	1	242	388	4.1	2.7
P11t	10.5	1	97	410	12.5	9.1
P11h	10.8	0.95	93	402	4.8	3.9
P11h-d	10.8	0.96	93	405	4.3	4.1

[a] XRD analysis indicated pure anatase phase.
[b] Primary particle size was calculated from XRD line broadening.
[c] I_0 for P5h and P11t was used as reference for P5 and P11 TiO_2, respectively.
[d] The reaction rates were calculated after steady-state condition was established.

TiO_2 exhibit a clear shift in the band-gap energy toward higher energy compared to the P11 TiO_2 (cf. Table 1). The Ti K-edge X-ray absorption near-edge spectra (XANES) and extended X-ray absorption fine structure (EXAFS) analyses of the P11 and P5 samples provide additional information on the local atomic environment, that is not available from X-ray diffraction. The XANES results shown in Fig. 1b indicate that the relative amount of 5-fold coordinated Ti (i.e., peak A2 at 4970.5 eV) is greater in P5 than in P11, which consist mostly 6-fold coordinated titanium atoms (i.e., peak A3 at 4971.75 eV). The postedge region of commercial anatase TiO_2 (i.e., 4980 to 5020 eV) contains a number of resolved and understood intense 3s→np dipole-allowed transitions that are also present in P11 but are absent in P5 samples. The EXAFS analysis done using UWXAFS 3.0 software package and FEFF8 program (Fig. 1c) shows that the amplitude of the Fourier transform of the Ti K-edge k^3-weighted EXAFS data (not corrected for phase shift) for P11 is higher than P5, especially for the peaks that correspond to the outer shells. The fitting results indicate that whereas the P11 TiO_2 display the characteristic four short and two long Ti–O bonds of an octahedral anatase TiO_2, the smaller P5 consist of three short (1.93 Å) and three long (1.98 Å) Ti–O bonds. The Ti K-edge EXAFS results are summarized in Table 2.

Table 2
Ti K-edge EXAFS results for TiO_2 catalysts

Samples	Shell	R (Å)	C.N.	σ^2 (Å^2)$\times 10^{-3}$
TiO_2	Ti–O	1.94	4.3	6.7
(commercial)	Ti–O	1.99	2.1	6.8
	Ti–Ti	3.07	3.5	4.6
	Ti–Ti	3.81	3.5	4.7
P5	Ti–O	1.94	2.8	8.9
	Ti–O	1.99	3.2	9.1
	Ti–Ti	3.05	2.2	5.9
	Ti–Ti	3.79	1.0	6.1
P11	Ti–O	1.95	3.9	7.8
	Ti–O	2.00	2.3	7.9
	Ti–Ti	3.06	3.3	5.3
	Ti–Ti	3.81	3.0	5.4

The high concentration of low coordinated Ti^{4+} cations, as well as the distorted anatase crystal structure observed in P5 TiO_2, suggests the possible presence of amorphous materials in these samples. However, a recent EPR study [7] was unable to detect the broad Ti^{3+} signal from the P5 sample, which is the main signal found in UV-irradiated amorphous TiO_2. The EPR data did confirm the presence of low coordinated Ti^{4+} cations but mostly on the crystal surface. This is understandable since the P5 TiO_2 contain a larger interfacial region where nearly 60% of its 17,600 TiO_2 units reside on the crystal surface compared to only 5% for P11 TiO_2. Since the surface Ti^{4+} sites are associated mostly with corner, step, edge, kink, and defect sites, this suggests that the smaller P5 TiO_2 have a rougher surface structure compared to P11. The subsurface Ti^{4+} associated with bulk defects was also detected indirectly from the formation of subsurface O^- species ($O_B{}^-$) when the P5 sample was irradiated in the presence of oxygen. The abundant surface hydroxyl groups on the P5 TiO_2 helped stabilize the photogenerated holes (h^+) at subsurface O^{2-} anion (i.e., $-O^{2-}-Ti^{4+}-OH + h^+ \rightarrow -O^- - Ti^{4+} - OH$). The XANES, EXAFS, and EPR experiments indicated that the smaller P5 TiO_2 do not only have a rougher and more hydrated surface, but also possess more bulk defects than the P11 TiO_2.

The P11 TiO_2 crystallized by thermal (P11t) and hydrothermal (P11h) processes have different EPR spectra. The spectra, obtained over the UV-irradiated P11t and P11h samples after their outgassing in vacuum ($T = 298$ K, $t =$ 1 h), displayed low intensity signals that suggest rapid recombination of photogenerated charges (i.e., e^- and h^+). The P11t spectrum consisted of several overlapping signals (i.e., g values > 2) that originated from oxygen radical species, while the P11h displayed a main signal that corresponds to Ti^{3+} cations in an anatase environment (i.e., $g_\perp = 1.991$ and $g_\parallel = 1.960$). The stabilization of the photogenerated electrons as Ti^{3+} cations on hydrothermally crystallized TiO_2 (e.g., P11h) is an indication of a rough surface that has an abundant number of Ti^{4+} sites in the form of defects, edges, and corners [8]. Their absence in P11t suggests that this catalyst possesses a smooth surface where electrons can remain delocalized in the conduction band. More information about the catalyst structure could be deduced from the EPR spectra of the UV-irradiated P11t and P11h samples

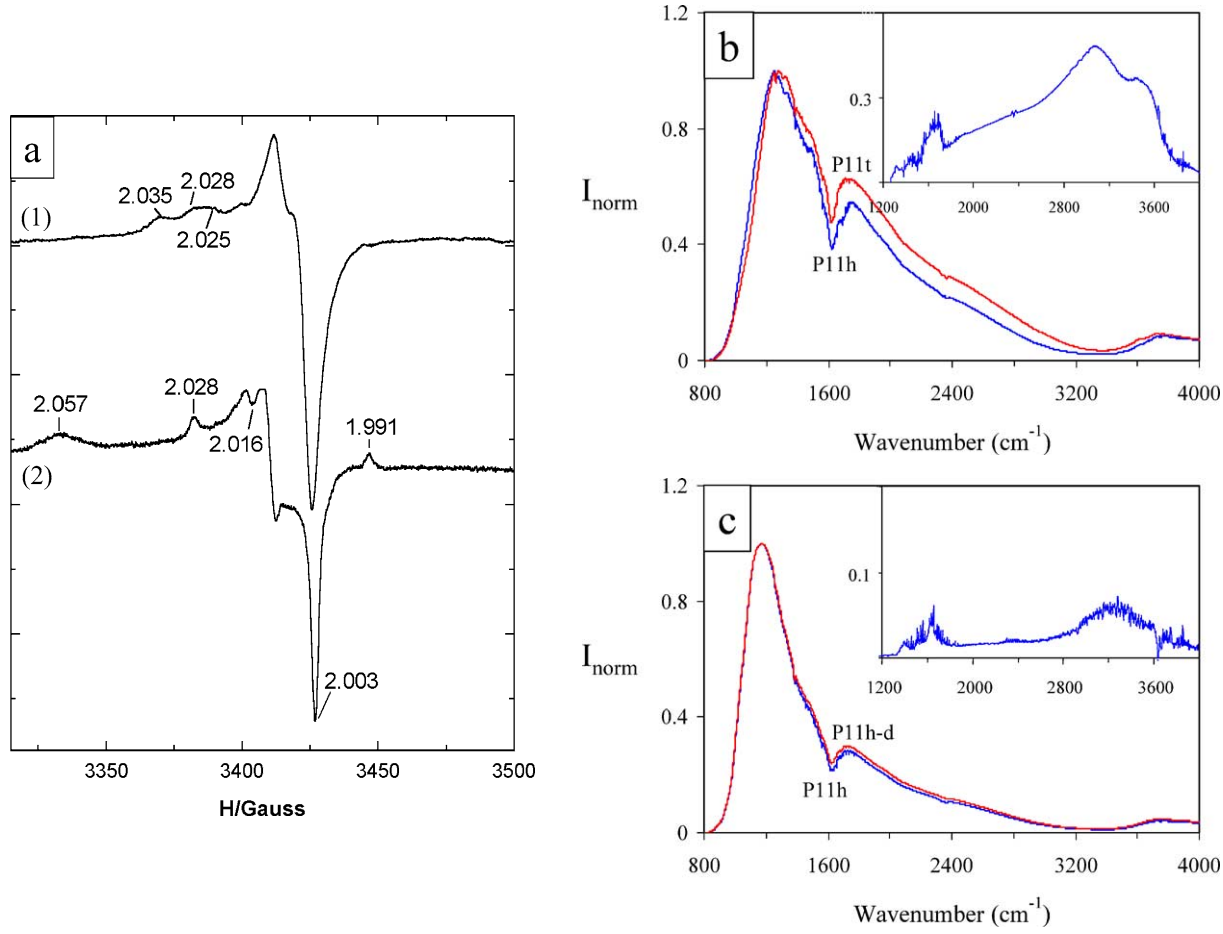

Fig. 2. (a) Electron paramagnetic spectra of UV irradiated (1) P11t and (2) P11h in the presence of adsorbed oxygen. FTIR transmittance spectra of (b) P11t and P11h and (c) P11h and P11h-d TiO_2.

in the presence of adsorbed oxygen (Fig. 2a). Since oxygen is a very efficient electron scavenger, its presence decreases the rate of annihilation of e^-–h^+ pairs and consequently, a larger number of radicals could be identified and studied.

Computer simulation indicates that the P11t spectrum consists of four main signals (Fig. 2a,1). They are O1 ($g_1 = 2.028$, $g_2 = 2.009$, $g_3 = 2.003$), O2 ($g_1 = 2.035$, $g_2 = 2.009$, $g_3 = 2.003$), O3 ($g_1 = 2.028$, $g_2 = 2.016$, $g_3 = 2.002$), and O4 ($g_1 = 2.011$, $g_2 = 2.007$, $g_3 = 2.003$). The O1 and O2 signals have been assigned to O_2^- and $OH_2\cdot$ that originated from the photogenerated electrons, whereas the O3 and O4 correspond to the surface O^- and O_3^- formed by the photogenerated holes. Computer deconvolution reveals that the P11h spectrum (Fig. 2a,2) is made of the overlapping O3 and O5 ($g_1 = 2.057$, $g_2 = 2.012$, $g_3 = 2.003$) signals. The O3 signal disappears from the P11h due to dipolar broadening after the addition of an excess amount of oxygen, without affecting the signal O5. It can be concluded that the species responsible for the O5 signal must be located within the bulk of anatase TiO_2 where it is inaccessible to oxygen. Signals with similar g_2 and g_3 values had been assigned to O^- species in bulk anatase (O_B^-); however, the g_1 value should have been lower than 2.057. Nakaoka and Nosaka [23] assigned the components at $g = 2.012$ and 2.003 to O_B^- species, and proposed that the $g = 2.057$ feature belongs to O_2^- (low field component) or water-related species (high field). However, our computer simulation results seem to indicate that the maximum at $g = 2.057$ must be a component of the orthorombic signal O5. Since this signal was observed mainly in the TiO_2 samples with very small crystal size where the presence of bulk defects is very likely, it must be related to O_B^- formed at these defect sites. It is believed that the feature at $g = 2.057$ corresponds to the geometry of the defect where O_B^- is located. From the EPR data, it can be concluded that hydrothermally crystallized P11h has a rougher surface and greater amounts of bulk defects than P11t.

Figs. 2b and c display the transmittance infrared spectra of P11t, P11h, and P11h-d TiO_2 after purging in dry air at room temperature for 2 h. The figure insets are the difference spectra. The spectra of P11t and P11h shown in Fig. 2b are the typical anatase TiO_2 spectra reported in the literature. It consists of a strong signal at about 1620 cm^{-1} that correspond to molecularly adsorbed water, a broad band at around 3400 cm^{-1} belonging to weakly bound water molecule and associated hydroxyl groups [24,25], and a peak centered at

3700 cm^{-1} assigned to isolated hydroxyls [24,26,27]. The sharp drop in transmission at around 1200 cm^{-1} is a characteristic feature of TiO_2, which has an intense absorbance at 980 cm^{-1}. The spectrum shown in the figure inset clearly shows that P11h, with its rougher surface rich in low coordinated titanium atoms, is able to harbor more hydroxyl groups and water than P11t. The P11h-d TiO_2 sample was obtained by UV irradiation of P11h to partially remove some of the surface bound water (Fig. 2c). Indeed, the figure inset shows that the UV irradiation of the TiO_2 results in a decrease of signal intensity at 1640 and 3400 cm^{-1} regions. The FTIR results show that the amount of surface-bound water and hydroxyl groups decreases from P11h to P11h-d and P11t. Both FTIR and EPR analyses of the P11 sample indicate that the three nanostructured TiO_2 have different surface properties. A similar study indicates that P5h-d obtained after the UV-mediated outgassing possessed a less hydrated surface compared to P5h. It can be summarized that in term of the surface roughness and bulk defects, P5h $\sim$ P5h-d $>$ P11h $\sim$ P11h-d $>$ P11t, and for the degree of surface hydration, P5h $>$ P5h-d and P11h $>$ P11h-d $>$ P11t.

3.2. Photocatalytic activity of nanostructured TiO_2

The performance of P11 and P5 nanostructured TiO_2 catalysts has been evaluated in a traditional, flat-plate photoreactor. The outlet gases were analyzed using gas chromatography from which the reaction rates were calculated (Table 1). Both the higher band-gap energy and greater number of bulk defects contribute toward the poorer mineralization rate of P5 photocatalyst. Although gas chromatography is a convenient method for most reaction studies, it is unable to provide real-time monitoring of the transient events that are occurring on the catalyst surface. This study employed an in situ Fourier-transform infrared spectroscopy to obtain information on the adsorbed species (i.e., reactants, intermediates, and products) and chemistry of the catalyst surface during the reaction [15]. Figs. 3a–c display time-series FTIR spectra for TCE photooxidation on P11t, P11h, and P11h-d, respectively. Prior to UV illumination ($t = 0$), the adsorbed TCE molecule displays characteristic bands at 850 ($\delta_{C–H}$), 950 ($\nu_{C–Cl}$), 1250 ($\delta_{CH–Cl}$), 1550 ($\nu_{C=C}$), 1580 ($\nu_{C=C}$), and 3070 cm^{-1} ($\nu_{C–H}$) [21]. Upon irradiation, the intensity of TCE bands (e.g., 850, 950, and 3070 cm^{-1}) exhibits a monotonic decrease with time, while the signals corresponding to CO_2 (i.e., 2340 and 2360 cm^{-1}), dichloroacetaldehyde (i.e., 1250 ($\delta_{C–H}$), 1400 ($\delta_{CH=O}$), and 1740 cm^{-1} ($\nu_{C=O}$) [15]), and formaldehyde (i.e., 1400 cm^{-1} ($\delta_{CH=O}$)) increase as the reaction progresses. Although the postreaction analysis of the catalyst surface reveals the presence of dichloroethylene band at 1600 cm^{-1} ($\nu_{C=C}$) and a weaker dichloroacetaldehyde band at 1250 cm^{-1} ($\delta_{C–H}$), these bands are obscured by water and TCE during the reaction. The gas chromatography detected three major reaction products from the photooxidation of TCE over the P11 catalysts. They are carbon dioxide, dichloroacetaldehyde, and dichloroethylene.

Fig. 4 plots the characteristic bands of TCE (950 cm^{-1}), CO_2 (2340 cm^{-1}), dichloroacetaldehyde (1745 cm^{-1}), and water/bicarbonates/dichloroethylene (1640 cm^{-1}) as a function of irradiation time. Fig. 4a shows a monotonic decrease in the intensity of the IR signal at 950 cm^{-1} as trichloroethylene is consumed by photocatalytic oxidation over the UV-irradiated catalysts. Four sets of experiments consistently show that P11t is more active than P11h for TCE conversion. The figure also shows that the irradiated P11h-d has a comparable activity as P11h. The carbon dioxide signal at 2340 cm^{-1} increases as the reaction progresses as shown in Fig. 4b. It can be seen from the figure that P11t is the most active of the three catalysts for photomineralization of TCE followed by P11h. The latter is only slightly worse in performance than P11h-d. Dichloroacetaldehyde is formed rapidly on P11h (Fig. 4c), quickly reaching an almost constant value early in the reaction (i.e., 20 min), whereas the amount of dichloroacetaldehyde formed on P11t is considerably less and takes a longer time (i.e., 90 min) to reach a maximum. An intermediate amount of dichloroacetaldehyde is found on P11h-d (Fig. 4c). The broad band with maximum at 1640 cm^{-1} (Fig. 4d) can arise from adsorbed water, formates, bicarbonates, and dichloroethylene ($\sim$ 1600 cm^{-1}). Although possible, the production of formates and bicarbonates during the photooxidation of TCE is unlikely. Adsorbed water is easily recognized by its distinct spectrum and its signal is weak even for the P11t catalyst that has the highest mineralization rate (cf. Fig. 3a). This suggests that the plots shown in Fig. 4d contain mainly the contribution from adsorbed dichloroethylene.

Besides monitoring the different adsorbed species formed during the reaction, the FTIR also reveals the changes in the surface properties of the TiO_2 catalyst. It is well known that the surface OH groups of TiO_2 play an important role in the photooxidation of organic compounds. By trapping photogenerated holes, the hydroxyl groups are transformed into reactive OH radicals that participate directly in the photooxidation reaction. They also serve as adsorption sites for organic molecules. Therefore, depending on the properties of their surface hydroxyl groups, the nanostructured TiO_2 can possess different photocatalytic activity. From the time-series FTIR spectra shown in Figs. 3b and c, it can be seen that the bands (i.e., 3600–3800 cm^{-1}) corresponding to isolated hydroxyls decrease with reaction time for P11h and P11h-d. This decrease suggests that these hydroxyl groups are either being transformed or consumed by the reaction. A similar decrease could also be due to strong adsorption of reaction intermediates or by-products on these hydroxyl groups. The lack of response in this region for P11t is most likely due to the absence of these hydroxyl groups from the TiO_2 that has been crystallized at high temperature.

A closer examination of Fig. 4a indicates that the initial TCE conversion rates of all three nanostructured TiO_2 are nearly the same. However, the more hydrated P11h ca-

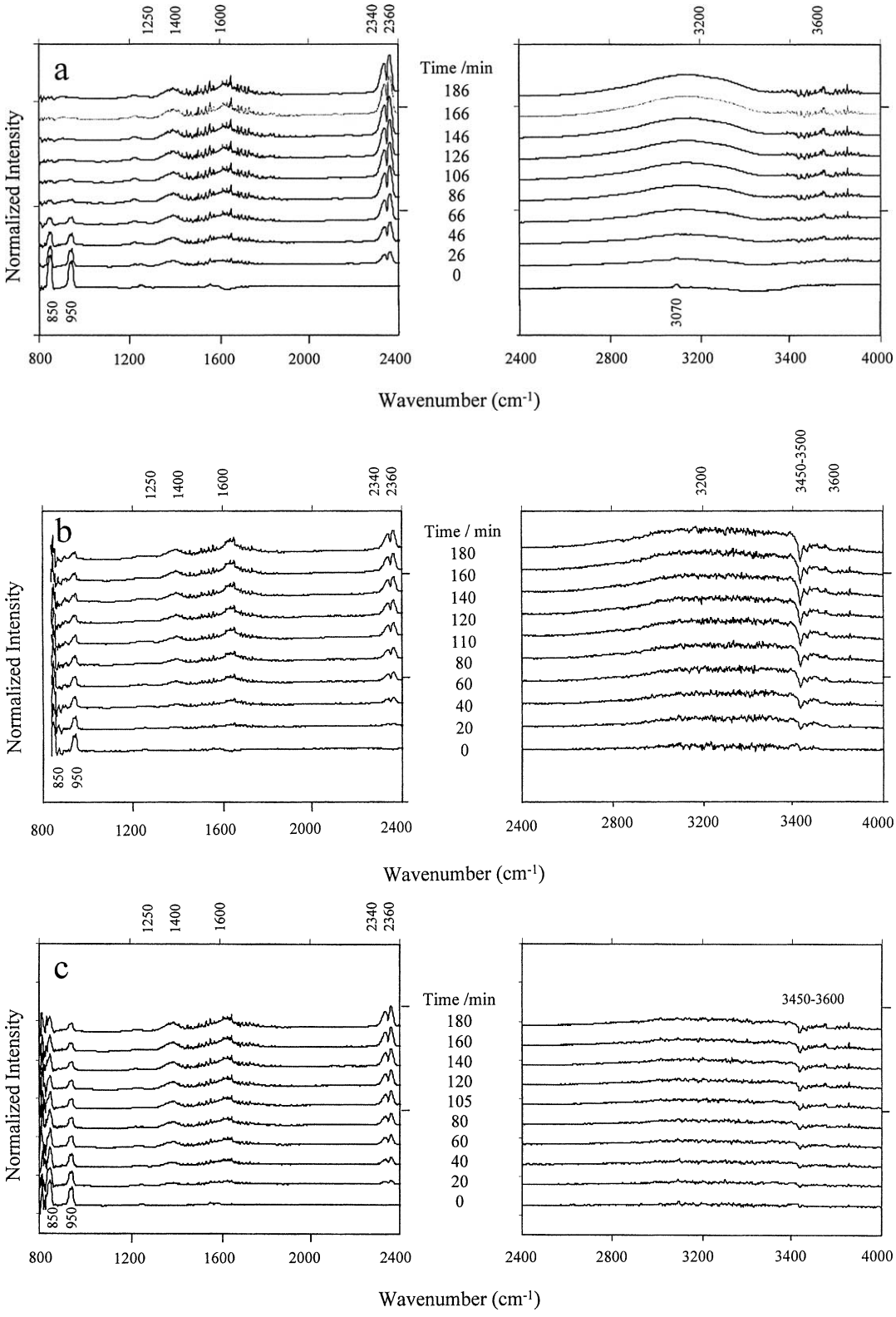

Fig. 3. FTIR spectra of TCE photooxidation on (a) P11t, (b) P11h, and (c) P11h-d as a function of UV irradiation time.

talyst produces mostly dichloroacetaldehyde (Fig. 4c) and dichloroethylene (Fig. 4d), which are strongly adsorbed on the TiO_2 surface such that the postreaction treatments in flowing dry air and UV irradiation were unable to completely remove them. Removing some of the surface hydroxyl groups by UV irradiation leads to less dichloroacetaldehyde and dichloroethylene (cf. Fig. 4c and d, P11h-d). The quantity of dichloroacetaldehyde and dichloroethylene sta-

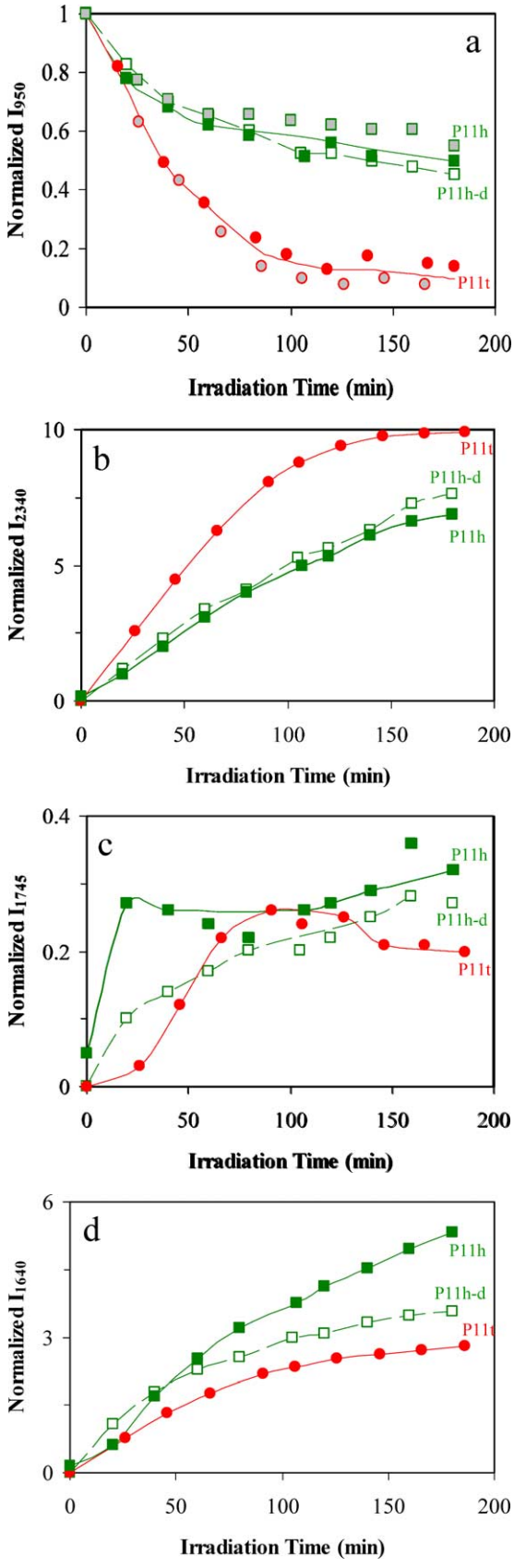

Fig. 4. Plots of the intensity of infrared signals from P11 TiO_2 corresponding to (a) TCE ($\nu_{C-Cl} = 950\ cm^{-1}$), (b) CO_2 (2340 cm^{-1}), (c) dichloroacetaldehyde, and (d) water/bicarbonates/dichloroethylene (1640 cm^{-1}).

bilized on P11t is significantly less than that of the other two TiO_2 catalysts. This strongly suggests that some of the surface hydroxyl groups present on the rough P11h and P11h-d catalysts are responsible for the production and stabilization of dichloroacetaldehyde and dichloroethylene compounds. The presence of these strongly adsorbed by-products on the catalyst can significantly decrease the number of surface sites available for the reaction, resulting in lower catalyst activity. This may explain the subsequent lower TCE conversion rates of P11h and P11h-d (Fig. 4a).

To verify that these sites are indeed responsible for the formation of dichloroacetaldehyde and dichloroethylene by-products, a smaller P5 TiO_2 catalyst was prepared. The smaller radius of curvature of P5 means that the catalyst surface consists mainly of edges, steps, and corners that are populated by low-coordinated titanium atoms. The P5h and P5h-d TiO_2 have similar structure, chemistry, and electronic state, but differ only in that P5h TiO_2 possesses a more hydroxylated surface compared to the UV-pretreated P5h-d TiO_2. Fig. 5 displays the plots of the characteristic IR bands for TCE, CO_2, dichloroacetaldehyde, and dichloroethylene as a function of reaction time. It is clear from the figure that the removal of hydroxyl groups from P5 TiO_2 leads to lower TCE conversion (Fig. 5a) due to the less production of dichloroacetaldehyde (Fig. 5c) and dichloroethylene (Fig. 5d). Indeed, only a trace amount of dichloroethylene could be found on P5h-d. The results of both photoreactor (Table 1) and in situ infrared reaction (Fig. 5b) studies indicate that P5h and P5h-d have comparable mineralization rates.

It can be deduced from the reaction data obtained from the two sets of nanostructured TiO_2 that the surface hydroxyl groups on low-coordinated titanium atoms are responsible for the formation of undesirable by-products from photooxidation TCE. The removal of these hydroxyl groups leads to a decrease in their production without affecting the mineralization reaction. This suggests that a different set of catalytic sites may be responsible for mineralization. There is also a strong correlation between mineralization efficiency and bulk defect densities, where catalysts containing more bulk defects exhibit lower mineralization. It can be concluded from this study that TiO_2 that has a rough and hydroxylated surface is a poor catalyst for TCE photomineralization. However, the same catalyst was found to be ideal for photomineralization of toluene [10]. In this case, the same hydroxyl groups serve as adsorption sites for toluene and catalyze the ring-opening reaction. Indeed, the toluene conversion rate over P11h catalyst is five times faster than on the P11t and unlike P11t, it does not produce benzoic acid [10].

4. Concluding remarks

This study demonstrates that the structure and chemistry of the nanostructured TiO_2 could be engineered using the modified sol–gel technique developed by the authors. The

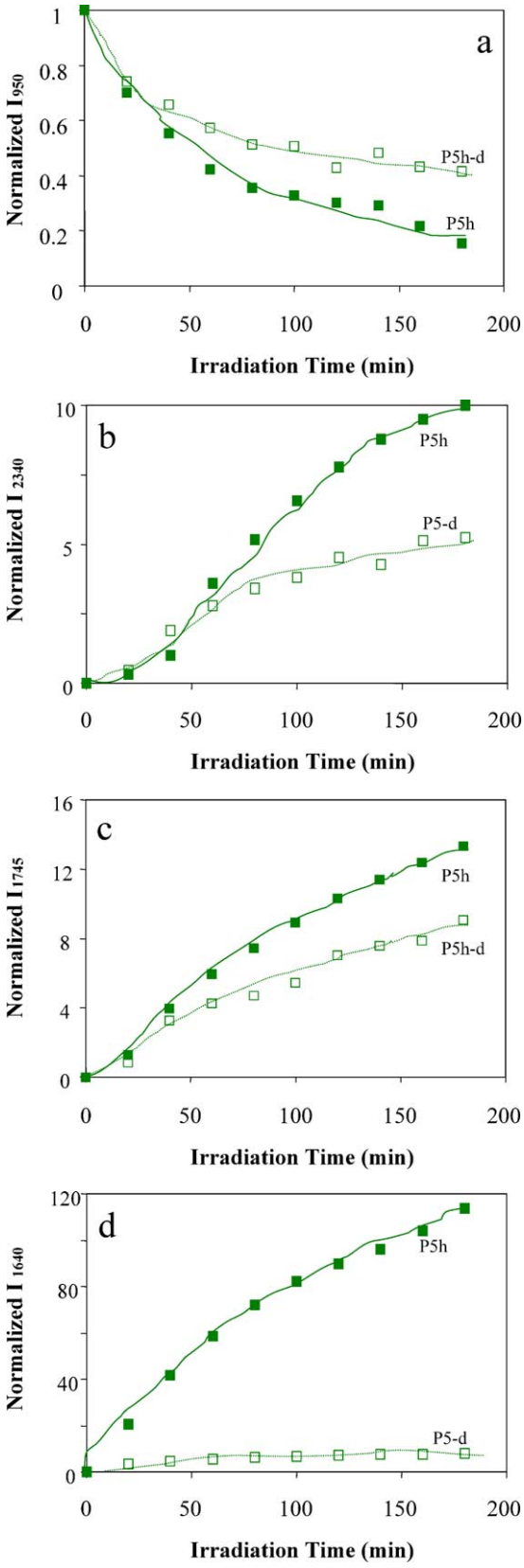

Fig. 5. Plots of the intensity of infrared signals from P5 TiO_2 corresponding to (a) TCE (ν_{C-Cl} = 950 cm^{-1}), (b) CO_2 (2340 cm^{-1}), (c) dichloroacetaldehyde, and (d) water/bicarbonates/dichloroethylene (1640 cm^{-1}).

size, crystallinity, and phase structure of the TiO_2 crystals as well as the aggregate size and shape could be precisely controlled using this preparation method. Manipulating the TiO_2's surface roughness and hydration allowed us to obtain catalysts with different surface properties. This ability enables us to study in more detail the role of surface properties on the photocatalytic activity of nanostructured TiO_2. Using the photooxidation of TCE as probe reaction, we were able to identify that the hydroxyl groups on low-coordinated titanium atoms are responsible for the generation of dichloroethylene and dichloroacetaldehyde by-products. These compounds are strongly adsorbed on the surface of TiO_2 and cannot be removed even after prolonged UV treatment in flowing air. Their presence usually means lower conversion and in cases leads to catalyst deactivation. This study also ascertained that there is a separate set of catalytic sites for mineralization reaction. Mineralization efficiency is low for TiO_2 catalysts that have higher band-gap energy or greater number of bulk defects. Most studies in the photocatalysis focus mainly on the bulk properties of the catalyst; this work clearly shows that a greater emphasis must be given to the surface properties of photocatalysts. A more detailed study is currently underway to identify the individual catalytic sites on nanostructured TiO_2 and to determine their role in the photoreaction.

Acknowledgments

The authors gratefully acknowledge the fundings from the Hong Kong Research Grant Councils (RGC-HKUST 6247/00P) and the Institute of Nano Science and Technology (INST). We also thank the Material Characterization and Preparation Facility (MCPF) at HKUST for the use of their FTIR.

References

[1] M.R. Hoffmann, S.T. Martin, W. Choi, D.W. Bahnemann, Chem. Rev. 95 (1995) 69.
[2] A.L. Linsebigler, G. Lu, J.T. Yates, Chem. Rev. 95 (1995) 735.
[3] M.A. Fox, T. Dulay, Chem. Rev. 93 (1993) 341.
[4] A.J. Maira, J. Soria, V. Augugliaro, V. Loddo, Chem. Biochem. Eng. Q. 11 (1997) 89.
[5] L. Cao, A. Huang, F.J. Spiess, S.L. Suib, J. Catal. 188 (1999) 48.
[6] A.J. Maira, K.L. Yeung, C.Y. Yan, P.L. Yue, C.K. Chan, J. Catal. 192 (2000) 185.
[7] A.J. Maira, K.L. Yeung, J. Soria, J.M. Coronado, C. Belver, C.Y. Lee, V. Augugliaro, Appl. Catal. B 29 (2001) 327.
[8] J.M. Coronado, A.J. Maira, J.C. Conesa, V. Augugliaro, J. Soria, Langmuir 17 (2001) 5368.
[9] A. Henglein, Chem. Rev. 98 (1989) 1861.
[10] A.J. Maira, J.M. Coronado, V. Augugliaro, K.L. Yeung, J.C. Conesa, J. Soria, J. Catal., in press.
[11] S. Yamazaki-Nishida, K.L. Nagano, L.A. Phillips, S. Cervera-March, M.A. Anderson, J. Photochem. Photobiol. A 70 (1993) 95.

[12] W.A. Jacoby, M.R. Nimlos, D.M. Blake, Environ. Sci. Technol. 28 (1994) 1661.
[13] S.A. Larson, J.L. Falconer, Appl. Catal. B 4 (1994) 325.
[14] L.A. Dibble, G.B. Raupp, Catal. Lett. 4 (1990) 345.
[15] L.A. Phillips, G.B. Raupp, J. Mol. Catal. 77 (1992) 297.
[16] L.A. Dibble, G.B. Raupp, Environ. Sci. Technol. 26 (1992) 492.
[17] W.A. Zeltner, C.G. Hill, M.A. Anderson, Chemtech 27 (1993) 21.
[18] M.R. Nimlos, W.A. Jacoby, D.M. Blake, T.A. Milne, Environ. Sci. Technol. 27 (4) (1993) 732.
[19] W.A. Jacoby, M.R. Nimlos, D.M. Blake, R.D. Noble, C.A. Koval, J. Catal. 157 (1995) 87.
[20] S.-J. Hwang, C. Petucci, D. Raftery, J. Am. Chem. Soc. 120 (1998) 4388.
[21] M.D. Driessen, A.L. Goodman, T.M. Miller, G.A. Zaharias, V.H. Grassian, J. Phys. Chem. B 102 (1998) 549.
[22] O. D'Hennelzel, D.F. Ollis, J. Catal. 167 (1997) 118.
[23] Y. Nakaoka, Y. Nosaka, J. Photochem. Photobiol. A 110 (1997) 299.
[24] C.J. Morterra, J. Chem. Soc., Faraday Trans. 84 (1988) 1617.
[25] M. Primet, P. Pichat, M.-V. Mathieu, J. Phys. Chem. 75 (1971) 1216.
[26] G. Cerrato, L. Marchese, C. Morterra, Appl. Surf. Sci. 70/71 (1993) 200.
[27] K. Kanaka, J.M. White, J. Phys. Chem. 86 (1982) 4708.